PERFORMANCE OF THE 2 MeV MICROWAVE GUN FOR THE SSRL 150 MeV LINAC*

M. Borland,[‡] M. C. Green,[◁] R. H. Miller,[◇] L. V. Nelson,[◁] E. Tanabe,[◇,◁] J. N. Weaver,[‡] and H.Wiedemann[‡]

[◇] AET Associates, Cupertino, CA 95014

[‡] Stanford Synchrotron Radiation Laboratory, Stanford University, Stanford, CA 94309

[◇] Stanford Linear Accelerator Center, Stanford University, Stanford, CA 94309

[◁] Varian Associates, Palo Alto, CA 94303

Abstract

As described previously,[1] the pre-injector linac for SSRL's 3 GeV synchrotron is fed by a 2 MeV, 1.5 A, low-emittance microwave gun, consisting of a thermionic cathode mounted in the first cell of a 1-1/2-cell S-band cavity. In this article, we report the successful operation of the gun, the longitudinally-bunching α-magnet, and the three-microbunch FET-pulsed beam-chopper. Simulations predict a normalized rms emittance at the gun exit of $< 10\ \pi \cdot m_e c \cdot \mu m$; chromatic effects in transport optics increase this to $\lesssim 30\ \pi \cdot m_e c \cdot \mu m$. The gun has a longitudinal phase-space suited to magnetic compression, as a result of which we predict that peak currents > 300 A in a 1 ps bunch are feasible.

Gun Design Overview

The SSRL RF gun was designed in collaboration by SSRL, AET Associates, and Varian Associates. The gun design had a number of goals, which were chosen not only with the needs of the SSRL Injector in mind, but also with the intention of producing a high-brightness electron source. These goals were: (1) For a cathode current density $J \leq 100$ A/cm^2, each bunch injected into the linac should contain 10^9 usable electrons; i.e., electrons with momenta $\geq 80\%$ of the peak momentum. (2) Peak momentum of 2 to 3 MeV/c for peak, on-axis electric fields in the second cell < 120 MV/m. (3) Near-linear, monotonic dependence of momentum p(t) on exit-time for 20-40 ps during a bunch, in order to allow magnetic bunch compression. (4) Gently converging beam in the gun for a wide range of current densities ($J < 100$A/cm^2). (5) Normalized rms emittance, $\epsilon_x \equiv \pi\left(\langle x^2\rangle\langle p_x^2\rangle - \langle x \cdot p_x\rangle^2\right)^{1/2}$ for the useful beam [as defined in goal (1)] of $< 15\pi \cdot m_e c \cdot \mu m$. (6) Manageable (i.e., < 5 W average at 10 pps for a 2 μs pulse) back-bomdardment power due to electrons returning to hit the cathode.

Figure 1 shows a cross-sectional view of the gun, which consists of a demountable, 6 mm diameter thermionic cathode in the first cell of a 1-1/2-cell S-band cavity. In order to thermally isolate the cathode from the metal walls of the cavity, the annular focusing structure around the cathode is also a thermal barrier made from metallized ceramic. RF electrical contact between this structure and the cathode is obtained using a toroidal tungsten-wire spring around the cathode stem.

The assumptions of design goal (1) turned out to be conservative in terms of the current density needed. The limiting factor was the RF power available to the gun. Obtaining beam momenta of the level desired implies cavity wall losses of about 1 MW. It was anticipated that about 4 MW total RF power would be available, implying 3 MW for the beam. For average kinetic energy 2 MeV, this implies that 1.5 A (3.3×10^9 e$^-$ per bunch) could be accelerated, requiring $J \approx 30$ A/cm^2. In order to obtain a match to the RF source under these conditions, the normalized load impedance without beam was chosen to be $\beta = 4$.

To satisfy goals (2) and (3), it was necessary to alter the excitation ratio of the two cells from the usual one-to-one ratio. In particular, the excitation level of the second is ≈ 2.9 times that of the first. This permits the gun to be operated over a wide range of gradients without obtaining the sinusoidal p(t) curve that appears when particles arrive in the second cell ahead of the crest. If one characterizes the excitation level of the gun in terms of the peak, on-axis electric field at the RF crest in the second cell, E_{p2}, then operation in the range $50\text{MV/m} < E_{p2} < 90\text{MV/m}$ (giving maximum momentum between 1.3 MeV/c and 3.3 MeV/c) produces a beam compatible with magnetic compression. Higher excitation yields more efficient extraction of beam, resulting in higher currents for the same current density.

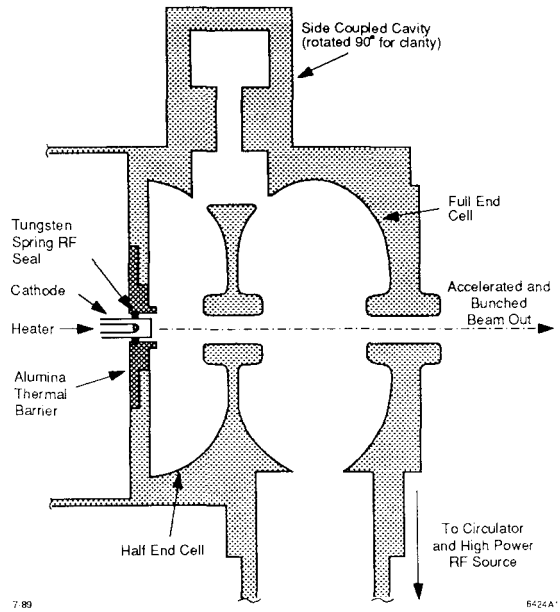

Fig. 1. Cross section of the gun cavity.

The shape of the focusing structure was arrived at using MASK[8] in order to satisfy design goals (4) and (5). The shape of the cavities themselves was not altered appreciably from that used for Varian medical linacs. Simulation details are reported elsewhere.[1,9]

As for goal (6), it was found that back-bombardment power would exceed 5 W average for $J \gtrsim 50$ A/cm^2 for the nominal gradient of $E_{p2} = 75$ MV/m. Fortunately, it is not necessary to use such high current densities in our application.

Operating experience with the gun to date indicates that the design goals have been largely met. Specifics of the longitudinal and transverse phase-space characterization are presented below. Here we offer a few general comments. Stable currents of up to 1.65 A have been obtained with ≈ 3.5 MW power, though the current installation does not provide sufficient RF power to exceed ≈ 900 mA. While back-bombardment is in evidence, it is a minor effect, permitting effective control of current via cathode filament power. The cathode currently in the gun has been run for about 300 hours with no sign of degradation.

*Work supported by Department of Energy contract DE–AC03–76SF00515.

Presented at the Linear Accelerator Conference, Albuquerque, New Mexico, September 10–14, 1990.

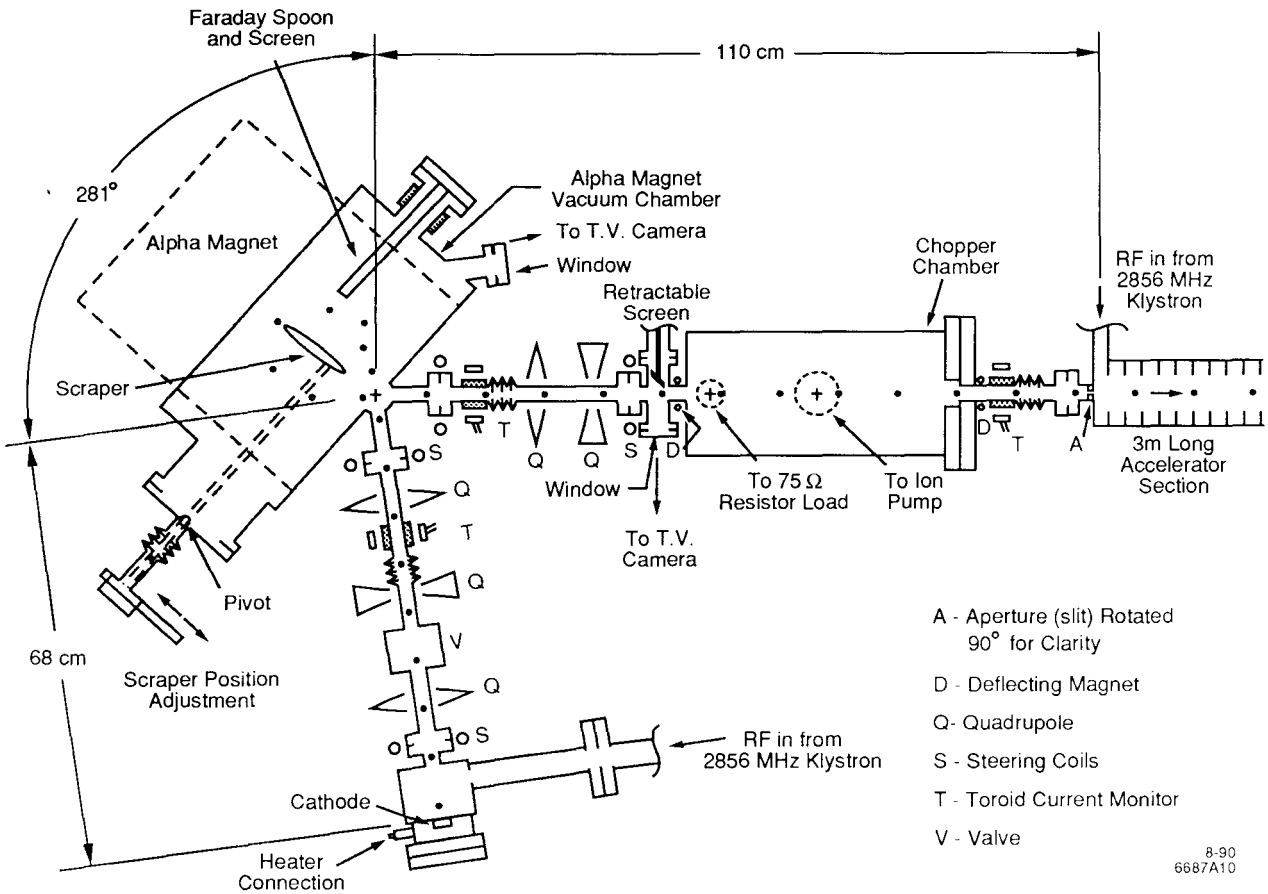

Fig. 2. Gun-to-linac layout.

Gun-to-Linac Transport Line

The Gun-to-Linac transport line ("GTL line"), shown schematically in Fig. 2 serves four main functions. The GTL line provides bunching of the beam in order to match to the longitudinal acceptance of the linear accelerator, and allows filtering out low-momentum particles. These functions are achieved using an α-magnet.[10] Quadrupoles and steering dipoles control the beam size and trajectory. The quadrupoles are required as part of the momentum filter (for good resolution), and to match the beam to the transverse acceptance of the accelerator, while providing a well-focused beam for proper operation of the chopper. The FET-pulsed beam-chopper permits the injection into the linac of only three S-band bunches of the several thousand that emerge from the gun during the RF pulse.

Magnetic Bunch Compression

The principle of magnetic bunching is to use a beamline with momentum-dependent path length. An additional requirement is zero dispersion at the end of the beamline, to avoid increasing the beam-size due to energy spread. Finally, momentum filtration requires nonzero dispersion at a location where an obstruction can be moved into the beam. All of these requirements can be satisfied with a system containing an α-magnet.[10]

The beam from the gun has a near-linear, monotonic dependence of exit time on momentum: $t_{exit}(p) \approx t_o + (dt_{exit}/dp)_o\ (p - p_o)$, where $p \equiv \beta\gamma$. To bunch the beam, all particles of interest must arrive at the linac at the same time. For reasonably small momentum spread, one can expand to first order in momentum deviation, and obtain the bunching condition:

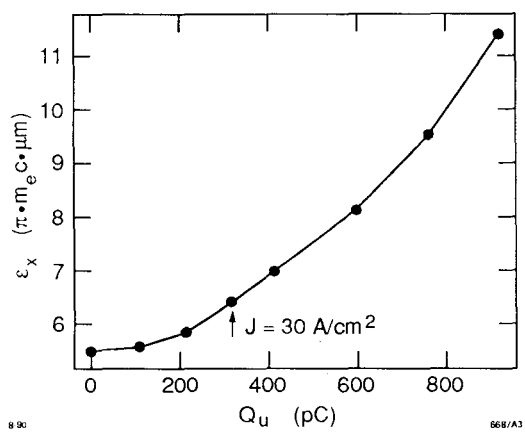

Fig. 3. Emittance versus charge per bunch.

$$\nabla B_\alpha = \frac{p_o K_\alpha^2 [\beta_o - 1/(2\beta_o)]^2}{\{cp_o(dt_{exit}/dp) + L_{drift}[\beta_o - (1/\beta_o)]\}^2},$$

where the constant $K_\alpha = 4.64210\ (m_e c/e)^{1/2}$ (MKS), was determined by numerical integration.[9]

Transverse Phase-Space

Figure 3 shows the predicted, normalized rms emittance in each plane for the "useful" beam (as defined above) at the gun exit, as a function of charge in the beam obtained through variation of the current density, from MASK simulations with $E_{p2} = 75$ MV/m. Note that the actual

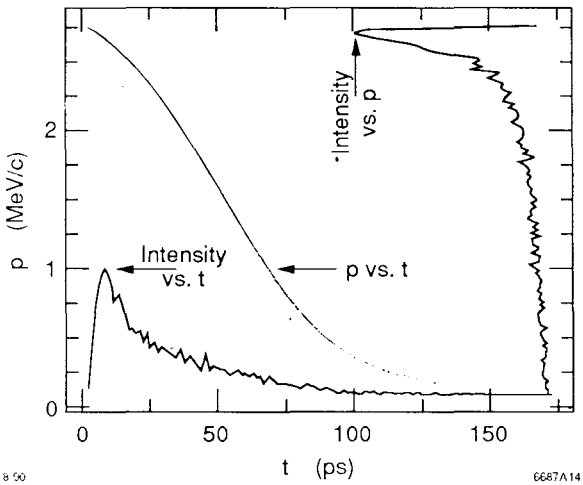

Fig. 4. Gun longitudinal phase-space.

emittance at the end of the GTL line is predicted to be significantly greater because of quadruople chromatic aberrations, and because we use ±10% momentum spread. In addition, since the beam is fully coupled, one can obtain significantly smaller emittance in one plane at the expense of the other plane. Hence, it is better to use the geometric mean, $\bar{\epsilon} = (\epsilon_x \epsilon_y)^{1/2}$ of the emittances in the two planes. Simulations predict that for $E_{p2} = 75$ MV/m, $\bar{\epsilon}$ at the end of the GTL is $\lesssim 30\ \pi \cdot m_e c \cdot \mu m$ for $J \leq 40$ A/cm^2, with only a weak dependence on current density, due in part to the overriding effect of chromatic abberations (compare Fig. 3).

The insertable screen before the beam-chopper can be used in conjunction with the quadrupole after the α-magnet to make measurements of the beam size versus the quadrupole strength. This data can be used to deduce the emittance. Measurements give horizontal emittances between 35 and 40 $\pi \cdot m_e c \cdot \mu m$. Future work will report on the emittances for both planes.

Longitudinal Phase-Space

Figure 4 shows MASK longitudinal phase-space results for $E_{p2} = 75$MV/m and J = 10A/cm^2. For a wide range of gradients, the longitudinal phase-space is characterized by a near-linear, monotonic dependence of momentum on exit-time. The momentum distribution is well-peaked near the maximum momentum and the particles are similarly bunched in time. In general, about 50% of the particles exiting the gun are within 20% of the maximum momentum, and these same particles extend over about 25 ps. For higher currents at the same gradient, the momentum peak is broader, as expected from the mutual repulsion of electrons in the beam; roughly speaking, one might find as much as a factor of two broadening in going from J = 10 to 40 A/cm^2.

Spectrum measurements can be made using a moveable scraper in the α-magnet, together with toroids before and after the α-magnet. Given such measurements, one can make various comparisons with simulations. For example, one can look at the dependence of the position of the momentum peak on the gradient. There are no field probes in the gun, so the gradient must be deduced from power conservation. The beam power can be inferred from the spectrum measurement, with account taken of losses in the transport line. Following this procedure, one can obtain an experimental relationship between the position of the momentum peak and the gradient. For "low-current" (i.e., < 100 mA average), we obtain reasonable agreement with simulations.

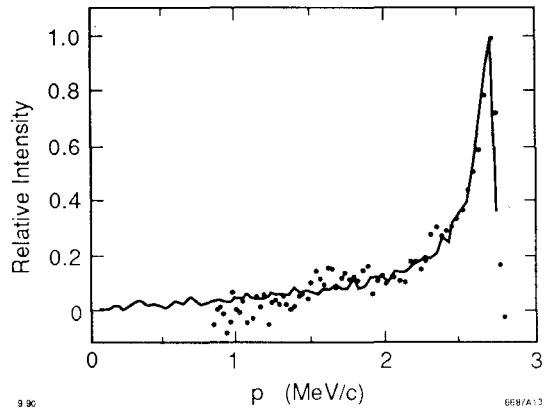

Fig. 5. Measured and simulated momentum spectra.

High-current (i.e., > 100 mA) experimental data seem to indicate that the actual power going into electrons is about twice what can be accounted for based on measurements of beam power transmitted through the α-magnet; possible explanations under investigation are secondary electrons,[11] detector diode calibration errors, stray magnetic fields, and transverse RF fields due to coupling slots.

One can also compare measured momentum distributions to calculated momentum distributions by matching the peaks of the distributions. Because of the space-charge effect mentioned just above, this is subject to the ambiguity of not knowing the current density. However, this does not become important until $J \gtrsim 30$ A/cm^2. A comparison between measured and simulated spectra is shown in Fig. 5.

Simulations predict that it is possible to obtain bunch lengths of 1 ps. For a gradient of 75 MV/m and J = 10 A/cm^2, a peak-current of 125 A is predicted, with 6×10^8 e$^-$ per bunch and $\bar{\epsilon} = 22\ \pi \cdot m_e c \cdot \mu m$. If J is increased to 40 A/cm^2, this becomes 347 A, with 2.3×10^9 e$^-$ per bunch and $\bar{\epsilon} = 23\ \pi \cdot m_e c \cdot \mu m$.

While this latter operating condition requires more RF power than currently available, the former operating condition has been achieved and exceeded, though the bunch length (and hence the peak current) has not been measured. Future experiments will measure the bunch length.

Acknowledgments

The authors wish to acknowledge the following people for design and engineering contributions: M. Baltay, B. Youngman (SSRL), R. McIntyre (VA). The following individuals provided technical and experimental support: C. Chavis, L. Emery, P. Golceff, J. Haydon, R. Hettel, B. Lavender, H. Morales, D. Mostowfi, J. Safranek, J. Sebek, D. Wang, C. Wermelskirchen (SSRL), W. Leong, S. Skellenger, and R. Tol (VA).

References

1. E. Tanabe *et al.*, SLAC-PUB-5054 (1989).
2. T. I. Smith, Proc. 1986 Linac Conf., pp. 421–426.
3. R. Miller *et al.*, Proc. 1986 Linac Conf., pp. 144–147
4. J. S. Fraser, Proc. 1986 Linac Conf., pp. 411–415.
5. G. A. Westenskow *et al.*, Laser and Particle Beams 2, Pt. 2, 223–5 (1984).
6. R. L. Sheffield *et al.*, NIM, 222–226 (1988).
7. K. T. McDonald, IEEE **QE–23**, 1489–96 (1987).
8. A. T. Drobot *et al.*, IEEE Trans. **NS–32**, 2733–7 (1985).
9. M. Borland, Ph.D thesis, Stanford Univ., to be published.
10. H. A. Enge, Rev. Sci. Instrum. **34**, No. 4, 385–389 (1963).
11. R. L. Sheffield, private communication.